Optics Letters

Slow light enabled high-modulation-depth graphene modulator with plasmonic metasurfaces

Tangxuan Ren and Lin Chen*

Wuhan National Laboratory for Optoelectronics, Huazhong University of Science and Technology, Wuhan 430074, China
**Corresponding author: chen.lin@mail.hust.edu.cn*

Received 6 September 2019; revised 1 October 2019; accepted 16 October 2019; posted 17 October 2019 (Doc. ID 377216); published 6 November 2019

Graphene has attracted the interest of researchers seeking to develop compact optical modulators with the flexible tunability of graphene conductivity by tuning the Fermi level. Plasmonic structures have provided a robust way to enhance the modulation depth (MD) of graphene optical modulators, but the available schemes suffer from low MD, fabrication complexities, or both. Here, an ultra-thin plasmonic metasurface structure capable of guiding slow surface plasmons (SPs) is proposed to construct graphene-based optical modulators. The designs take advantage of the strong field enhancement of slow SP modes as well as the orientation match between the electric field and the graphene plane. A typical 0.96-μm-long metasurface-based graphene modulator presents a significantly improved MD of 4.66 dB/μm and an acceptable insertion loss of 1.4 dB/μm, while still having ease of fabrication.

https://doi.org/10.1364/OL.44.005446

High-speed, ultra-compact, and power-efficient optical modulators are of great importance for on-chip optical interconnects. Silicon optical modulators have been heavily studied over the past few years, but the footprint is typically in millimeters due to silicon's weak electro-optical properties [1]. While promising steps have been taken to integrate silicon modulators with high-quality-factor optical resonators, the resultant optical modulators suffer from intrinsic narrow bandwidth and stringent optical design [2]. Graphene is distinctive and appealing for its high electron mobility, wide operation bandwidth, and electric tunability of conductivity by gating. Inspired by these outstanding properties, graphene has attracted a great deal of attention in developing active optoelectronic devices, including photodetectors [3] and dedicated sensors [4].

The optical absorption of graphene can be tuned effectively by changing the chemical potential of graphene, E_f. Therefore, graphene also has been widely explored to construct compact high-performance optical modulators [5–16]. A graphene-based broadband optical modulator on the SOI platform was successfully realized by electrically tuning the Fermi level of a monolayer graphene sheet [5]. Since this pioneering work, much effort has been devoted to optimizing the design to enhance the modulation depth (MD). By adding two-layer graphene on the silicon waveguide, a nearly doubled MD of 0.16 dB/μm can be obtained [6]. However, the enhancement of the MD is limited due to the intrinsically weak electric field at the interface between the designed dielectric waveguide and graphene. To address this issue, it has been proposed to insert a graphene layer into the dielectric waveguide, where the electric field of waveguide mode is at maximum [17]. However, this design faces significant fabrication challenges and has not yet been demonstrated experimentally.

Surface plasmons (SPs) are evanescent waves bounded at a metal/dielectric interface, with the parallel wavevectors being larger than the free-space value [18–20]. SPs can squeeze a light field into a deep subwavelength scale, which significantly enhances electric field intensity. Combining SP structures with graphene points out a promising way to develop high-efficiency graphene modulators with an ultra-compact footprint. Initially, by utilizing corrugated and wedge SP structures, graphene-based SP modulators were experimentally demonstrated with a MD in 10^{-4} dB/μm [7]. The MD with the plasmonic structure is small and even lower than those with silicon waveguide-based optical modulators. The cause of low modulation efficiency originates from the orientation mismatch between the SP field and graphene plane. It is therefore not surprising that the researchers have turned to enhancing the interaction by exploiting SP structures that are able to convert the orientation of a major component of the electric field of SPs to the graphene plane [8–11,13–16]. While the MD is significantly improved to 0.4–4 dB/μm with the assistance of various plasmonic structures, the preparation of them, including groove-structured metallic gratings [8], multilayer graphene [15], hybrid plasmonic waveguides [11,13,14], and metal nanoparticles coupled with silicon waveguides [10,16] would increase fabrication cost and complexity in practice. Therefore, it is of great value to exploit novel plasmonic structures that not only can achieve high MD, but also can relax the fabrication difficulty.

In this Letter, we demonstrate that an ultra-thin plasmonic metasurface structure is capable of guiding SPs with the orientation of the major component of the electric field of SPs being parallel to the graphene plane. Moreover, by properly optimizing the geometries of the metasurfaces, the dispersion relation of SP modes can be well engineered to reduce the

group velocity of SP modes. The resultant graphene modulator presents significantly improved MD due to the enhanced interaction between the slow SP modes and graphene.

As shown in Fig. 1, the proposed metasurface-based graphene modulator consists of a gold rod array on top of a single sheet of graphene. The gold rod has length a, width w, and thickness t_m along the x, y and z directions, respectively, and the lattice constant of the array along the x direction is denoted as d. It is known that the conventional SP mode has its main electric field component oriented along the normal direction to the metal surface. For a single column of gold antennas along the x direction, both the air and the dielectric layers underneath the antennas contribute to propagating SP mode, with the electric field component being oriented along the x, y, and z directions [21,22]. For the gold rod array, the coupling of SP modes between the adjacent columns of gold antennas significantly enhance the electric field (especially for the Ey component), depending on the spacing, as denoted as g in Fig. 1. When a single sheet of graphene with the thickness of $t_g = 0.34$ nm is placed underneath the metasurface, the orientation direction of the SP field matches well with the graphene plane. Hence, it is supposed to enhance the SP-graphene interaction. A bias voltage assumedly applies between the graphene layer and a 50-nm-thick, shallow-doped silicon layer deposited on a silica substrate, spaced by an Al_2O_3 layer with a thickness of 10 nm. Therefore, we can have the variable E_f for graphene by dynamically tuning the bias voltage. The thickness of the silicon layer is designed to have a larger electric field at the Al_2O_3/air interface [Fig. 2(a)], which is beneficial for increasing the MD.

The dispersion curve of the SP mode by the proposed metasurface structure can be obtained by the finite-difference time-domain (FDTD) method with the commercial software *Lumerical FDTD Solutions*. Here we fix a at 100 nm, w at 100 nm, t_m at 30 nm for the gold rod antennas, and d at 200 nm. Figure 2(b) shows that, as frequency increases, the propagation constant increases sharply, and the dispersion curve deviates significantly from the light line (black solid line), suggesting the emergence of propagating slow SP modes. The propagation constant of the SP mode can be tuned by either changing the geometry of the gold rod antennas (discussed later) or modulating the spacing along the y direction. Reducing the spacing will render the cutoff frequency of slow SP modes lower. Figures 2(c)–2(f) reveal that the effective wavelength of the SP mode gradually reduces as g decreases, suggesting a significant reduction of the group velocity of the SP modes. Apparently, the E_y component of the SP mode is the dominating field component as E_y is larger than E_z. In addition, the field intensity of the SP mode is significantly enhanced as g is tuned to make the light frequency approach the cutoff frequency of the SP mode, associated with a reduction of group velocity. Besides, the modulation effect of graphene is closely related to the magnitude of the in-plane electric field, where the graphene plane is located. Figures 2(g) and 2(h) demonstrate that the electric field is more concentrated at the bottom of the metasurface. This indicates that it is better to place graphene underneath the metasurface than on top of the metasurface to maximize the SP-graphene interaction. The design takes advantage of the strong field enhancement of the slow SP mode as well as the orientation match between the electric field of the slow SP mode and the graphene plane. These two factors are expected to enhance the graphene-light interaction, and significantly improve the MD.

When a single graphene layer is placed underneath the metal rods, the SP modal profiles experience a gentle variation, but their propagating loss can be significantly influenced by the gate voltage applied on graphene, V_g, associated with E_f. The in-plane conductivity of graphene, σ, versus E_f is calculated using the Kubo formula [23]. The in-plane permittivity of graphene is expressed as $\varepsilon = 1 + i\sigma/\omega\varepsilon_0 t_g$, with ε_0 the permittivity of air and ω the angular frequency of light. The influence of V_g on E_f is related to the carrier density, n, as $E_f = \hbar V_f(\pi n)^{1/2}$ and $n = \varepsilon_0\varepsilon_d V_g/et_d$, where $\hbar(= h/2\pi)$ is the reduced Planck constant, V_f ($\approx 10^6$ m/s) is the Fermi velocity, e is the charge of an electron, t_d (=10 nm) represents the thickness of the Al_2O_3 layer, and ε_d (=9) is the RF dielectric constant of Al_2O_3. Figures 3(a) and 3(b) show the in-plane conductivity and permittivity of graphene versus E_f, where the carrier mobility of graphene, μ, is 3000 $cm^2/(V \cdot s)$, associated with the scattering rate of 3.7 meV and 2.2 meV at $E_f = 0.3$ eV and 0.5 eV, respectively. The out-of-plane permittivity of graphene is kept at 2.5.

As E_f is below the threshold ($\hbar\omega/2 = 0.4$ eV, associated with $V_g = 2.4$ V), the electron interband transition occurs

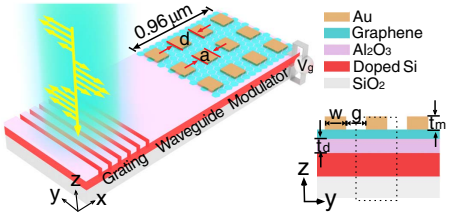

Fig. 1. Schematics of the graphene modulator based on metasurfaces consisting of gold rod antennas. The cross-section of the modulator in the y – z plane is shown in the right side. The SP mode can be excited by using gratings that normally couple y-polarized light into the dielectric waveguide connecting gratings and metasurfaces. The whole device is assumed to be infinite along the y direction.

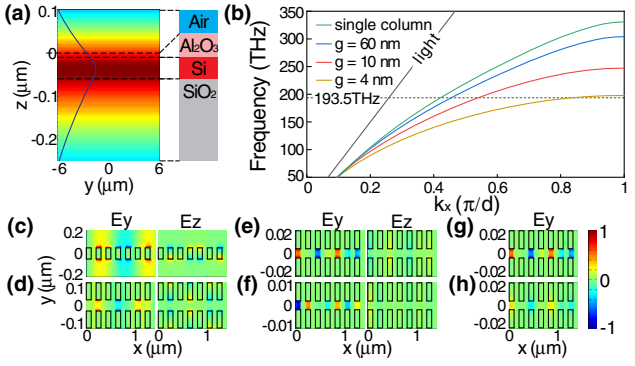

Fig. 2. (a) Distributions of Ey magnitude for the TE mode in the silicon waveguide. (b) Dispersion curves of SP modes supported by gold rod antennas for different geometric parameters. (c)–(f) The real part of E_y and E_z field distributions at the bottom of gold rod antennas at $\lambda = 1550$ nm for (c) a single column with $w = 100$ nm, (d) $w = 100$ nm, $g = 60$ nm, (e) $w = 100$ nm, $g = 10$ nm, and (f) $w = 100$ nm, $g = 4$ nm. (g)–(h) The real part of E_y field distributions at the bottom (g) and top (h) of the metasurfaces with $w = 100$ nm and $g = 10$ nm. (d)–(h) show the zoomed view of electric field distributions between two adjacent columns of gold nanorods.

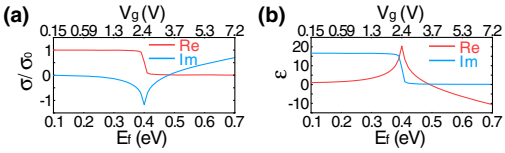

Fig. 3. (a) Real and imaginary parts of in-plane conductivity and in-plane permittivity. (b) Real and imaginary parts of in-plane conductivity of graphene as a function of E_f at 1550 nm. σ_0 (=60.8 μS) is the universal optical conductance.

associated with a large absorption loss. When V_g exceeds 2.4 V, graphene appears to be nearly transparent with an extremely low loss since no electron is available for the interband transition. When $E_f = 0.3$ eV ($V_g = 1.3$ V), and 0.5 eV ($V_g = 3.7$ V), the proposed structure in Fig. 1 suffers from high and low attenuation, respectively, and the applied voltage difference, ΔV_g, is 2.4 V. To quantitatively evaluate the performance of the metasurface modulator, the figure of merit (FOM) is defined as FOM = MD/IL (IL is the abbreviation for insertion loss) [9]. The influence of the thickness with different dielectric materials (SiO_2, hBN, and Al_2O_3) on the modulator performances is shown in Figs. 4(a) and 4(b). Using the same dielectric material, the MD decreases as the thickness increases, while the FOM has an inverse tendency. The utilization of the dielectric material with a higher refractive index will result in higher MD and lower FOM due to higher insertion loss. To get a low bias voltage, a 10-nm-thick layer of Al_2O_3 is chosen as the spacer due to its largest ε_d among the three materials. Then, how the length, a, and the period, d, affect the device performances is considered. With the definition of duty cycle (F) as a/d, the dependence of the modulator performance on F is shown in Figs. 4(c) and 4(d), where d is set at 100 nm and 200 nm. Both the attenuation and the MD increase with F. Nevertheless, the FOM changes slightly when $F < 0.5$ and decreases significantly when $F > 0.5$, due to the fact that the growth rate of the MD is smaller than the growth rate of IL as F exceeds 0.5. Hence, F is fixed at 0.5 to optimize the modulator performances. As for the different period, d, the

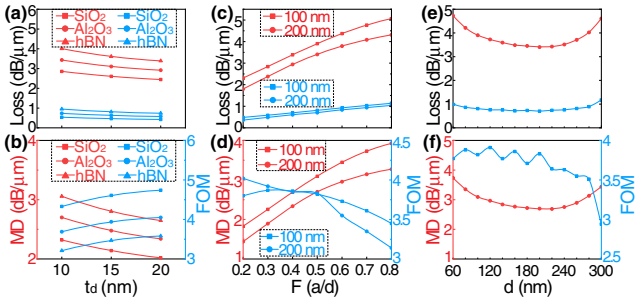

Fig. 4. (a) Loss at 0.3 eV and 0.5 eV and (b) MD and FOM as a function of t_d with SiO_2, hBN, and Al_2O_3. The refractive indices of SiO_2, hBN, and Al_2O_3 are 1.44, 1.98, and 1.75, respectively. The spacing, g, is fixed at 10 nm, while the other geometrical parameters are the same as those in Fig. 2. (c) Loss at 0.3 eV and 0.5 eV and (d) MD and FOM as a function of duty cycle F. (e) Loss at 0.3 eV and 0.5 eV and (f) MD and FOM as a function of period d. The other geometrical parameters in (c)–(f) are the same as those in (a) and (b). The red and blue lines in (a), (c), and (e) represent 0.3 eV and 0.5 eV, respectively.

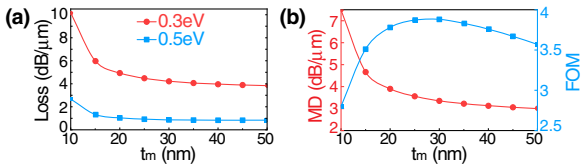

Fig. 5. (a) Loss at 0.3 and 0.5 eV as a function of t_m. (b) MD and FOM as a function of t_m. a and d are fixed at 40 nm and 80 nm, respectively, while w and g are the same as those in Fig. 4. The dielectric spacer is a 10-nm-thick Al_2O_3 layer.

attenuation and the MD are at their minimums at approximately $d = 200$ nm, but they increase as d approaches 60 nm and 300 nm [Figs. 4(e) and 4(f)]. The FOM oscillates within a wide range of d, and the maximum value occurs at approximately $d = 120$ nm. The FOM at $d = 120$ nm is slightly larger than that at $d = 80$ nm, while the MD at $d = 80$ nm is much larger than that at $d = 120$ nm. Therefore, d is fixed at 80 nm for the metasurface-based graphene modulator design. Next, the influence of t_m on the performance is considered. Figure 5 shows that the MD decreases as t_m increases from 10 nm to 50 nm and the largest FOM is found at approximately $t_m = 30$ nm. The FOM at $t_m = 30$ nm is slightly larger than that at $t_m = 25$ nm, while the MD at $t_m = 25$ nm is much larger than that at $t_m = 30$ nm. Therefore, a thickness of $t_m = 25$ nm is chosen to optimize the metasurface-based graphene modulator in the following.

As has been stated in Fig. 2, a highly confined and enhanced slow SP mode can be obtained by reducing g to increase the coupling strength of SP modes. In addition, w can be increased to enhance the electric field of the slow SP mode (not shown here). However, these two methods for the electric field enhancement of the SP mode suffer from increased propagation loss, which can be verified by the propagation loss versus g and w, as shown in Figs. 6(a) and 6(b). The MD shares the same tendency with the propagation loss, i.e., it is increased with the reduction of g and the increment of w [Fig. 6(c)]. It should be noted that, there exists an azure region at the bottom of each figure, representing the SP band gap, i.e., the SP mode is forbidden to travel with these geometrical parameters. For a fixed w, the maximum MD appears as light frequency approaches the edge of the SP bandgap, but the corresponding propagation loss is maximized as well. A high MD of 7.17 dB/μm and a FOM of 3.64 can be achieved at (g, w) = (3 nm, 70 nm). However, the high-aspect-ratio gap between the adjacent nanorods will increase manufacturing difficulty. To compromise the modulator performance and future experimental feasibility, the geometric parameters (g, w) = (10 nm, 110 nm) can be chosen,

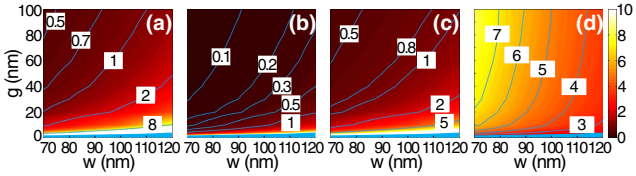

Fig. 6. (a) Loss at 0.3 eV and (b) loss at 0.5 eV for different w and g. (c) MD and (d) FOM for different w and g. The solid lines labeled with numbers represent the contour lines. a, d, and t_m are fixed at 40 nm, 80 nm, and 25 nm, respectively, while the dielectric spacer is a 10-nm-thick Al_2O_3 layer.

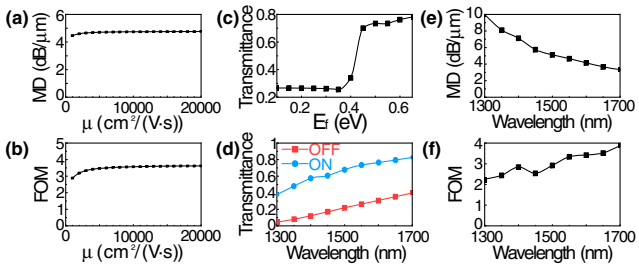

Fig. 7. (a) MD and (b) FOM as a function of carrier mobility. (c), (d) Transmission as a function of E_f (c) and wavelength (d). (e) MD and (f) FOM as a function of wavelength.

which produces a large MD of 4.66 dB/μm, an acceptable insertion loss of 1.4 dB/μm and a FOM of 3.34, respectively. The MD and the FOM are reduced to 0.85 dB/μm and 0.62, respectively, if graphene is placed above the metasurfaces.

Figures 7(a) and 7(b) reveal that the MD and the FOM change gently as μ varies from 1000 $cm^2/(V \cdot s)$ to 20000 $cm^2/(V \cdot s)$. The device performances versus light frequency with a 0.96-μm-long metasurface graphene modulator is then studied. The transmittance with respect to E_f at 1550 nm is shown in Fig. 7(c). In addition, graphene's high carrier mobility and strong optical absorption are independent of wavelength, suggesting the capability of working over a wide spectral range. The transmittance as a function of wavelength from 1300 nm to 1700 nm is depicted in Fig. 7(d). It is worth noting that the proposed metasurface structure presents high attenuation in the low wavelength region with $E_f = 0.5$ eV. To avoid this issue, the E_f is tuned to be 0.6 eV for the "ON" state in the wavelength region from 1300 nm to 1400 nm. The resultant metasurface modulator has a MD of more than 3 dB/μm from 1300 to 1700 nm [Fig. 7(e)].

Table 1 presents a list of the existing graphene modulators with various nanostructures. Compared with the schemes in Refs. [5–7], the subsequent graphene modulators overcome the orientation mismatch between the major electric field and graphene plane, resulting in a much larger MD [8,9,11,12,14–16]. Our proposed metasurface scheme further increases the MD by exploiting the slow SP mode to enhance the electric field, while maintaining an acceptable IL of 1.4 dB/μm. The FOM/ΔV_g is larger than most of the reported modulators due to the high FOM (3.34) achieved and low ΔV_g (2.4 V) used. It is also worth noting here that the fabrication of a one-layer ultra-thin plasmonic metasurface typically requires one-step electron beam lithography and the deposition of gold film, followed by a lift-off process. The preparation difficulty can be lower than these schemes with plasmonic waveguides [10,11,14–16] and high-aspect-ratio metallic grooves [8].

Table 1. Performance Comparison

Refs.	Length (μm)	MD (dB/μm)	IL (dB/μm)	FOM	FOM/ΔV_g	Result
[5]	40	0.1	–	–	–	Exp.
[6]	40	0.16	–	–	–	Exp.
[7]	12	0.03	–	–	–	Exp.
[8]	8	0.4	0.43	0.93	0.55	Sim.
[9]	3	1.2	1.6	0.75	0.3	Sim.
[11]	3.6	1.23	0.10	12.8	0.98	Sim.
[12]	40	0.62	–	–	–	Exp.
[14]	–	1.58	0.2	7.9	0.61	Sim.
[15]	10	1.76	0.21	8.46	2.56	Sim.
[16]	1.05	4	2.48	1.61	0.22	Sim.
ours	0.96	4.66	1.40	3.34	1.39	Sim.

In conclusion, an ultra-thin metasurface that enhances graphene absorption by virtue of the strong field enhancement of the slow SP mode and the orientation match between the electric field and the graphene plane is proposed. The resultant metasurface graphene modulator exhibits a significantly higher MD over a wide spectral range than previous optical modulators, while undergoing ease of fabrication and acceptable insertion loss. This design could inspire the construction of various nanophotonic devices with metasurfaces, with simultaneous SP field enhancement and SP field being oriented in-plane.

Funding. National Natural Science Foundation of China (11474116, 11674118).

Disclosures. The authors declare no conflicts of interest.

REFERENCES

1. R. A. Soref and B. R. Bennett, IEEE J. Quantum Electron. **23**, 123 (1987).
2. Q. F. Xu, B. Schmidt, S. Pradhan, and M. Lipson, Nature **435**, 325 (2005).
3. T. Mueller, F. N. A. Xia, and P. Avouris, Nat. Photonics **4**, 297 (2010).
4. Y. Y. Shao, J. Wang, H. Wu, J. Liu, I. A. Aksay, and Y. H. Lin, Electroanalysis **22**, 1027 (2010).
5. M. Liu, X. Yin, E. Ulin-Avila, B. Geng, T. Zentgraf, L. Ju, F. Wang, and X. Zhang, Nature **474**, 64 (2011).
6. M. Liu, X. B. Yin, and X. Zhang, Nano Lett. **12**, 1482 (2012).
7. D. Ansell, I. P. Radko, Z. Han, F. J. Rodriguez, S. I. Bozhevolnyi, and A. N. Grigorenko, Nat. Commun. **6**, 8846 (2015).
8. Y. L. Wang, T. Li, and S. N. Zhu, Opt. Lett. **42**, 2247 (2017).
9. Z. Ma, M. H. Tahersima, S. Khan, and V. J. Sorger, IEEE J. Sel. Top. Quantum Electron. **23**, 81 (2016).
10. P. Chang, C. Lin, and A. S. Helmy, Laser Photon. Rev. **11**, 1700003 (2017).
11. X. Peng, R. Hao, Z. Ye, P. Qin, W. Chen, H. Chen, X. Jin, D. Yang, and E. Li, Opt. Lett. **42**, 1736 (2017).
12. H. Shu, Z. Su, L. Huang, Z. Wu, X. Wang, Z. Zhang, and Z. Zhou, Sci. Rep. **8**, 991 (2018).
13. B. Huang, S. Gao, W. Lu, and Z. Liu, Opt. Express **26**, 7358 (2018).
14. R. Hao, Z. Ye, X. Peng, Y. Gu, J. Jiao, H. Zhu, E. Wei, and E. Li, IEEE Photon. J. **10**, 4500807 (2018).
15. Z. Wu and Y. Xu, Appl. Opt. **57**, 3260 (2018).
16. B. Wang, S. Blaize, J. Seok, S. Kim, H. Yang, and R. Salas-Montiel, IEEE J. Sel. Top. Quantum Electron. **25**, 4600706 (2019).
17. K. Kim, J. Y. Choi, T. Kim, S. H. Cho, and H. J. Chung, Nature **479**, 338 (2011).
18. W. L. Barnes, A. Dereux, and T. W. Ebbesen, Nature **424**, 824 (2003).
19. Y. Deng, J. Yu, M. Zhang, and L. Zhang, Front. Optoelectron. **10**, 138 (2017).
20. C. Wan, G. Rui, J. Chen, and Q. Zhan, Front. Optoelectron. **12**, 88 (2019).
21. X. Shen, T. J. Cui, D. Martin-Cano, and F. J. J. Garcia-Vidal, Proc. Natl. Acad. Sci. USA **110**, 40 (2013).
22. Z. Li, M.-H. Kim, C. Wang, Z. Han, S. Shrestha, A. C. Overvig, M. Lu, A. Stein, A. M. Agarwal, and M. Lončar, Nat. Nanotechnol. **12**, 675 (2017).
23. R. Amin, Z. Ma, R. Maiti, S. Khan, J. B. Khurgin, H. Dalir, and V. J. Sorger, Appl. Opt. **57**, D130 (2018).